Ocean Dynamics (2017) 67:973–988
DOI 10.1007/s10236-017-1068-x

Evolution of wave and tide over vegetation region in nearshore waters

Mingliang Zhang[1] · **Hongxing Zhang**[1] · **Kaibin Zhao**[1] · **Jun Tang**[2] · **Huifa Qin**[3]

Received: 6 February 2017 / Accepted: 8 May 2017 / Published online: 24 May 2017

Abstract Coastal wetlands are an important ecosystem in nearshore regions, where complex flow characteristics occur because of the interactions among tides, waves, and plants, especially in the discontinuous flow of the intertidal zone. In order to simulate the wave and wave-induced current in coastal waters, in this study, an explicit depth-averaged hydrodynamic (HD) model has been dynamically coupled with a wave spectral model (CMS-Wave) by sharing the tide and wave data. The hydrodynamic model is based on the finite volume method; the intercell flux is computed using the Harten–Lax–van Leer (HLL) approximate Riemann solver for computing the dry-to-wet interface; the drag force of vegetation is modeled as the sink terms in the momentum equations. An empirical wave energy dissipation term with plant effect has been derived from the wave action balance equation to account for the resistance induced by aquatic vegetation in the CMS-Wave model. The results of the coupling model have been verified using the measured data for the case with wave-tide-vegetation interactions. The results show that the wave height decreases significantly along the wave propagation direction in the presence of vegetation. In the rip channel system, the oblique waves drive a meandering longshore current; it moves from left to right past the cusps with oscillations. In the vegetated region, the wave height is greatly attenuated due to the presence of vegetation, and the radiation stresses are noticeably changed as compared to the region without vegetation. Further, vegetation can affect the spatial distribution of mean velocity in a rip channel system. In the co-exiting environment of tides, waves, and vegetation, the locations of wave breaking and wave-induced radiation stress also vary with the water level of flooding or ebb tide in wetland water, which can also affect the development and evolution of wave-induced current.

Keywords Wetland vegetation · CMS-wave · Hydrodynamic model · Wave attenuation · Tide-wave-vegetation interaction

Responsible Editor: Guoping Gao

✉ Mingliang Zhang
zhmliang_mail@126.com

[1] School of Ocean Science and Environment, Dalian Ocean University, Dalian, Liaoning 116023, China

[2] State Key Laboratory of Coastal and Offshore Engineering, Dalian University of Technology, Dalian, Liaoning 116023, China

[3] Panjin Pink Beach Travel Ltd, Panjin, Liaoning 124216, China

1 Introduction

The waves in offshore areas not only can cause damages to the buildings in coastal areas, but can also change the offshore water environment and affect the sediment bed deformation. The coastal wetland plants, such as *salt marshes* and *mangroves*, are key members of the coastal ecosystem. As a non-intrusive buffer, they play an important role in dissipating wave energy and protecting coastline from erosion (Moller et al. 1999; Feagin et al. 2011; Das and Crépin 2013; Anderson and Smith 2014). The potential of using these coastal plants as part of coastal protection has attracted researchers' interest and has been a hot research topic. The physical model and the numerical model are usually used in investigating the sea wave propagation and the flow movement over the plant field in order to understand the interactions of waves, currents, and vegetation. Some researchers had carried out many laboratory experiments to investigate the interactions between waves and vegetation (Lovas et al. 2000; Turker et al. 2006; Irtem et al. 2009, Hu et al. 2014; Maza et al. 2015). The

horizontal wave-induced drag forces of a stem array using a bulk drag coefficient C_d were frequently reported by researchers, such as Dubi and Torum 1997; Lovas et al. 2000; Méndez and Losada 2004. Several studies on numerical modeling of wave propagation over vegetation had been carried out to investigate the interaction of waves and the plants by solving the Reynolds Average Navier–Stokes equations (RANS) (Li and Yan 2007; Zhang et al. 2013; Ma et al. 2013; Marsooli and Wu 2014; Maza et al. 2016). In the investigations, the k-ε, k-ω, and the Spalart–Allmaras turbulent model accounting for vegetation-induced turbulence production were considered for turbulence closure in the RANS model. The wave attenuation induced by the vegetation was obtained in these studies. Based on the modified Boussinesq equations, Augustin et al. (2009) simulated the irregular wave propagation through the flexible vegetation in a shallow water wave basin using the Cornell University Long and Intermediate Wave (COULWAVE) model. Blackmar et al. (2014) applied a phase-resolving Boussinesq model (FUNWAVE) in predicting wave height attenuation through a heterogeneous stand of the two vegetation types. These studies derived the friction factors to account for the effects of vegetation (Augustin et al. 2009; Blackmar et al. 2014). The phase-averaged models were used to solve the wave energy balance equation or wave action equation in a frequency domain and were widely applied to large study areas; it accounted for the energy dissipation using a bottom friction term. The phase-averaged spectral model SWAN (Booij et al. 1999), which was modified for the study of wave transformations on the vegetation zone, is called SWAN-VEG (Chen and Zhao 2012; Suzuki et al. 2012). These models mentioned above simulated the wave height attenuation in the presence of vegetation, but the interaction of wave, current, and vegetation could not be investigated in the co-exiting environment wave and current. An exclusive wave model is necessary to couple with the shallow water flow model in order to simulate both the wave field and the wave-induced flow field. Much research effort had been applied to focus on wave-current interaction with a large variety of circulation models and wave models. 2-D coupling models for wave-current interaction were set up using depth- and wave period-averaged mathematical formulations of the mass, momentum, wave energy, and wave number conservation relations based on one-way approach (Luettich et al. 1992; Park and Borthwick 2001; Buttolph et al. 2006, Loder et al. 2009; Dietrich et al. 2012, Wang et al. 2014). A two-way coupling algorithm for wave-current interaction was also applied to the modeling system; it could share the information of tide and wave models of the coupling system in real time; the data of wave model were given into tide model, and the data of hydrodynamic model could be fed back to the wave model as input at an inner iteration loop (Zhang et al. 2012; Ding et al. 2013; Sanchez et al. 2016; Lawler et al. 2016); it is more reasonable than the one-way approach. Researchers had successfully developed the 3-D coupling models such as Coupled Ocean-Atmosphere-Wave-Sediment Transport (COAWST) (Warner et al. 2010; Kumar et al. 2012; Zeng et al. 2015), SWAN (Booij et al. 1999) + FVCOM (Qi et al. 2009; Kaveh et al. 2016; Chen et al. 2016), SWAN + ECOM-si (Blumberg 1994), and SWAN + Delft3D (Hansen et al. 2015) to simulate the circulation, sediment transport, and wave dynamics for regions characterized by irregular complex coastlines, islands, inlets, creeks, and intertidal zones. Moreover, some researchers had applied a coupling model to investigate the capacity of wetlands and coastal marshes to attenuate storm surge by changing the Manning coefficient for wetland domain in the hydrodynamic model (Lawler et al. 2016). Actually, the drag force approach considering vegetation parameters is more accurate for evaluating the wetlands' effect on the hydrodynamic and wave process.

Due to the lack of knowledge on the interactions among tides, waves, and wave-induced currents in wetland waters, especially on the wave energy dissipation and tide motion in the vegetated domain, it is of interest to understand the effects of rigid and flexible vegetation on the structure in a wave and current co-existing environment. The CMS-Wave model is a spectral wave model in the SMS Software developed by Coastal and Hydraulics Laboratory, USA (Lin et al. 2008). It has been coupled with an explicit 2-D shallow water hydrodynamic model in this study. The simulation results for regions with and without vegetation have been compared with corresponding measured data.

2 Wave model

In this study, the wave model (CMS-Wave) is based on the wave action balance equation. It takes into account the effect of wave breaking, shoaling, refraction, diffraction, wave-current interaction, and bottom friction. The wave energy loss induced by the vegetation is derived from the wave action balance equation in CMS-Wave, which can be expressed as follows:

$$\frac{\partial(C_x N)}{\partial x}+\frac{\partial(C_y N)}{\partial y}+\frac{\partial(C_\theta N)}{\partial \theta} = \frac{\kappa}{2\sigma}\left[\frac{\partial}{\partial y}\left(CC_g\cos^2\theta\frac{\partial N}{\partial y}\right)-\frac{CC_g}{2}\cos^2\theta\frac{\partial^2 N}{\partial y^2}\right]-\varepsilon_b N-Q_v-S \quad (1)$$

where x and y are the horizontal coordinates in two directions; N is the wave action density and is defined as the wave energy-density E divided by the relative angular frequency σ. θ is the wave direction, C is wave celerity. C_x and C_y are defined as $C_x = C_g\cos\theta + u, C_y = C_g\sin\theta + v$, C_g is the group velocity u and v are current velocity components in the x and y directions, respectively. A default value of $\kappa = 2.5$ is used for the diffraction intensity parameter as suggested by Mase

(2001). ε_b is the parameterization of wave breaking energy dissipation, S is the source terms (e.g., wind forcing, bottom friction loss, non-linear wave–wave interaction term), and Q_v is the source term due to vegetation effect.

C_θ is defined as

$$C_\theta = \frac{\sigma}{\sin 2kh}\left(\sin\theta\frac{\partial h}{\partial x} - \cos\theta\frac{\partial h}{\partial y}\right) + \cos\theta\sin\theta\frac{\partial u}{\partial x} - \cos^2\theta\frac{\partial u}{\partial y} + \sin^2\theta\frac{\partial v}{\partial x} - \sin\theta\cos\theta\frac{\partial v}{\partial y} \quad (2)$$

where k is the wave number, h is the water depth. The extended Miche formula is used for calculating the wave breaking term. The wave energy dissipation due to vegetation had been defined by Dalrymple et al. (1984). Méndez and Losada (2004) modified Dalrymple's formula to enable the estimation of the wave dissipation from vegetation in narrow-banded random waves. The wave height H was replaced by a root mean square wave height (H_{rms}) with the Rayleigh probability density function. Q_v is expressed as

$$Q_v = \frac{1}{\sigma 2\sqrt{\pi}}\rho C_d b_v N_v\left(\frac{kg}{2\sigma}\right)^3 \frac{\sinh^3(k\alpha h) + 3\sinh(k\alpha h)}{3k\cosh^3(kh)} H_{rms}^3 \quad (3)$$

where ρ is water density, C_d is drag coefficient of plant, b_v is the stem diameter of the cylinder (plant), N_v is the number of plants per square meter and g is the gravitational acceleration, α is the relative vegetation height (h_v/h), and h_v is the vegetation height. According to the relationship between E and N for the random wave energy, the vegetation source term can be written in terms of the wave action density, $Q_v = \varepsilon_v N$. Then, the coefficient ε_v is

$$\varepsilon_v = \frac{4}{g\sqrt{\pi}} C_d b_v N_v\left(\frac{kg}{2\sigma}\right)^3 \frac{\sinh(k\alpha h) + 3\sinh(k\alpha h)}{3k\cosh^3(kh)} H_{rms} \quad (4)$$

Bulk drag coefficient is dependent on the plant height, water depth, and the Keulegan–Carpenter number. Hence, the bulk drag coefficient varies with these parameters, and it has to be calculated at each calculation grid. Méndez and Losada (2004) concluded that C_d is a function of the relative depth of the plant and the Keulegan–Carpenter number, which is defined as

$$C_d = \frac{\exp\left\{-0.0138\left(K_v/(h_v/h)^{0.76}\right)\right\}}{\left(K_v/(h_v/h)^{0.76}\right)^{0.3}} \quad (5)$$

where $K_v = u_c T/b_v$, u_c is a characteristic velocity acting on the plant and defined as the maximum horizontal velocity at the top of the plant in each point of the vegetation field, and T is the wave period. The maximum horizontal orbital velocity is used to replace the maximum horizontal velocity at the top of the local plant in the simulations.

The wave action density N is solved by discretizing Eq. (1) using a forward-marching first-order upwind finite-difference method with a Cartesian grid (Mase 2001). It is expressed as follows:

$$A_1 N_n^{IJK} + A_2 N_n^{I(J-1)K} + A_3 N_n^{I(J+1)K} + A_4 N_n^{IJ(K-1)} + A_5 N_n^{IJ(K+1)} = B N_n^{(I-1)JK} \quad (6)$$

where I and J are the total grid numbers, and K and n are the total numbers of angular and frequency components, respectively. A_1, A_2, A_3, A_4, A_5, and B are the coefficient in the discretized equation; the TDMA (Tridiagonal Matrix Algorithm) is used to solve the discretized equation (Mase 2001). Boundary conditions such as an open sea boundary, a dissipative beach boundary, and a reflecting wall boundary are taken into account in this model. The capability of the CMS-Wave model had been verified to simulate the wave refraction, diffraction, and breaking over an irregular bed and in real coastal waters with good precision (Lin and Demirbilek 2005, Lin et al. 2008).

3 Nearshore current model

The numerical model used in this study consists of the 2-D shallow water equations describing the conservation of mass and momentum. The shallow water equation written in conservation and vector form is expressed as:

$$\frac{\partial U}{\partial t} + \frac{\partial E}{\partial x} + \frac{\partial G}{\partial y} = \frac{\partial E_d}{\partial x} + \frac{\partial G_d}{\partial y} + S_f \quad (7)$$

where $\boldsymbol{U}$ are the vectors of the conserved variables; $\mathbf{E}$, $\mathbf{G}$, $\mathbf{E}_d$, and $\mathbf{G}_d$ in Eq. (7) are the convection fluxes and the diffusion fluxes in the x and y directions, respectively. $\mathbf{S_f}$ is the source terms, which can be defined as follows:

$$U = \begin{bmatrix} h \\ hu \\ hv \end{bmatrix}, E = \begin{bmatrix} hu \\ huu \\ huv \end{bmatrix}, G = \begin{bmatrix} hv \\ huv \\ hvv \end{bmatrix}, E_d = \begin{bmatrix} 0 \\ \nu_t \frac{\partial uh}{\partial x} \\ \nu_t \frac{\partial vh}{\partial x} \end{bmatrix}, G_d = \begin{bmatrix} 0 \\ \nu_t \frac{\partial uh}{\partial y} \\ \nu_t \frac{\partial vh}{\partial y} \end{bmatrix}, S_f = \begin{bmatrix} 0 \\ -gh\frac{\partial \eta}{\partial x} - S_{Sx} - \tau_{bx} + f_c hv - f_x \\ -gh\frac{\partial \eta}{\partial y} - S_{Sy} - \tau_{by} - f_c hu - f_y \end{bmatrix} \quad (8)$$

where τ_{bx} and τ_{by} are the bed shear stress term with x and y components defined by the velocities, respectively, and η is the water level above the still water. The unit-width hu and hv are the conservative dependent variables, grouped in the column vector $\mathbf{U}$. S_{Sx} and S_{Sy} are the wave-induced radiation force term with x and y components, respectively, and f_c is the Coriolis parameter; ν_t is the eddy viscosity.

The drag force exerted on vegetation per unit volume can be expressed as:

$$f_x = \frac{1}{2}N_v C_d b_v \min(h_v, h) u\sqrt{u^2+v^2},\quad f_y = \frac{1}{2}N_v C_d b_v \min(h_v, h) v\sqrt{u^2+v^2} \tag{9}$$

The eddy viscosity, ν_t, is calculated by a weighted mixing coefficient as follows (Buttolph et al. 2006):

$$v_t = (1-D)\beta u^* h + D\Lambda u_m H \tag{10}$$

where D is the coefficient for the eddy viscosity defined by the wave height, H is wave height. $u_*$is the bed shear velocity defined as $u^* = [c_f(u^2+v^2)]^{1/2}$and $\beta$is an empirical coefficient between 0.3 and 1.0; Λ is the mixing parameter equal to 1.0; u_m is the amplitude of the horizontal component of the wave orbital velocity at the bottom. τ_{bx} and τ_{by} are defined under combined currents and waves, as follows (Buttolph et al. 2006):

$$\tau_{bx} = n^2 h^{-3/4}\left\{\left(U_{wc}+\frac{\omega_b^2}{U_{wc}}\cos^2\gamma\right)u + \left(\frac{\omega_b^2}{U_{wc}}\cos\gamma\sin\gamma\right)v\right\}$$
$$\tau_{by} = n^2 h^{-3/4}\left\{\left(\frac{\omega_b^2}{U_{wc}}\cos\gamma\sin\gamma\right)u + \left(U_{wc}+\frac{\omega_b^2}{U_{wc}}\cos^2\gamma\right)v\right\} \tag{11}$$

$$\omega_b = \frac{\sigma H}{\pi \sinh(k(d+\eta))} \tag{12}$$

where γ is the wave angle relative to the x-axis, n is the Manning's roughness coefficient, and U_{wc} is the near bed orbital velocity, d is the still water depth. In the case of simulating the wave-induced currents, the near bed orbital velocity has to be taken into account.

The wave orbital velocity, U_{wc} is given by:

$$U_{wc} = \frac{1}{2}\left\{\sqrt{\left|u^2+v^2+\omega_b^2+2(u\cos\gamma+v\sin\gamma)\omega_b\right|}+\sqrt{\left|u^2+v^2+\omega_b^2-2(u\cos\gamma+v\sin\gamma)\omega_b\right|}\right\} \tag{13}$$

The wave stress forces S_{Sx} and S_{Sy} are calculated using the following equations:

$$S_{Sx} = -\frac{1}{\rho}\left(\frac{\partial S_{xx}}{\partial x}+\frac{\partial S_{xy}}{\partial y}\right),\quad S_{Sy} = -\frac{1}{\rho}\left(\frac{\partial S_{xy}}{\partial x}+\frac{\partial S_{yy}}{\partial y}\right) \tag{14}$$

where S_{xx}, S_{xy}, and S_{yy} are the wave-driven radiation stresses; the calculations of the radiation stress tensor are based on linear wave theory.

The hydrodynamic model is based on the two-dimensional depth-averaged non-linear shallow water equations by using an unstructured and multiple-level quadtree mesh with local refinement for important region (Zhang et al. 2012), where all cells are numbered in a one-dimensional sequence using the fully unstructured approach. The non-staggered grid layout is applied to all the variables (velocity, water level, and water depth) located at the center of each grid element.

3.1 HLL scheme

The intercell flux is computed by the HLL approximate Riemann solver with shock captured capability for computing the dry-to-wet interface for coastline (Toro 2001; Zhang et al. 2013). The HLL scheme assumes and defines the flux at the interface as:

$$F_{HLL} = \begin{cases} F_L & \text{if } S_L \geq 0 \\ F^* & \text{if } S_L < 0 < S_R \\ F_R & \text{if } S_R \leq 0 \end{cases} \tag{15}$$

where $\mathbf{F}_L$ and $\mathbf{F_R}$ are the flux evaluated at the left-hand and right-hand sides of each cell interface. $\boldsymbol{F}^*$ denotes the flux at the intermediate state for the 2-D model, given by:

$$F^* = \frac{S_R F_L - S_L F_R + S_L S_R(U_R - U_L)}{S_R - S_L} \tag{16}$$

where $\mathbf{U}_L$ and $\mathbf{U_R}$ are the conservative variable vectors evaluated at the left-hand and right-hand sides of each cell, and S_L and S_R are the celerities of the waves at the left-hand and right-hand sides of each cell.

The wave celerities S_L and S_R can be estimated as follows:

$$S_L = \min\left(U_L - \sqrt{gh_L}, u^* - \sqrt{gh^*}\right) \tag{17}$$

$$S_R = \max\left(U_R + \sqrt{gh_R}, u^* + \sqrt{gh^*}\right) \tag{18}$$

where $u^* = \frac{1}{2}(U_L + U_R) + \sqrt{gh_L} - \sqrt{gh_R}$, $\sqrt{gh^*} = \frac{1}{2}\left(\sqrt{gh_L} + \sqrt{gh_R}\right) + \frac{1}{2}(U_L - U_R)$, and h_L and h_R are the water depths of the left-hand and right-hand sides of each cell,

respectively. For a dry bed situation, the wave speeds S_L and S_R are estimated according to the following expressions:

$$S_L = U_L - \sqrt{gh_L},\quad S_R = U_L + 2 \times \sqrt{gh_L} \text{ for right dry bed} \tag{19}$$

$$S_L = U_R - 2\sqrt{gh_R},\quad S_R = U_R + \sqrt{gh_R} \text{ for left dry bed} \tag{20}$$

If the intermediate states U_L and U_R are defined as the cell-centered values, a first-order accurate scheme can be obtained. However, it suffers from excess numerical dissipation, and accuracy is limited. Second-order spatial accuracy can be obtained by employing a Monotonic Upstream Scheme for Conservation Laws (MUSCL) reconstruction technique. For each cell, the limited gradient and reconstructed left and right states can be obtained and used to calculate the fluxes at the interfaces. These fluxes in turn can be used as inputs to the Riemann solver. Usually, a piecewise linear reconstruction is used in the x-direction, as follows:

$$U^L_{i+\frac{1}{2}} = U_i + \frac{\Delta x_i}{2}\left(\frac{\partial U}{\partial x}\right)_i \tag{21}$$

$$U^R_{i+\frac{1}{2}} = U_{i+1} + \frac{\Delta x_{i+1}}{2}\left(\frac{\partial U}{\partial x}\right)_{i+1} \tag{22}$$

The gradients across cell i are determined using the values in the neighboring cells $i + 1$. Such gradient calculations often result in undershoots or overshoots which cause spurious oscillations in the solution. Hence, the *minmod* slope limiter is used in the model so as to eliminate undershoots or overshoots (Toro 2001), and the limited gradients are calculated as follows:

$$\left(\frac{\partial U}{\partial x}\right)_i = \text{minmod}\left(\frac{U_i - U_{i-1}}{x_i - x_{i-1}}, \frac{U_{i+1} - U_i}{x_{i+1} - x_i}\right) \tag{23}$$

The dynamic coupling of the two models requires an exchange of the information in an iterative process. The wave model needs to provide the results of the radiation stresses, wave height, and wave period for the hydrodynamic model. Meanwhile, the water level and velocity results from the hydrodynamic model are used by the wave model.

4 Numerical studies

4.1 Random wave propagation in sloping beach with vegetation

Generally, in most coastal areas, real beach has a slight slope. Further, coastal wetlands, such as marshes and swamps, act as a natural shoreline protection against damages from storm surges and waves. In this case, the laboratory data of Lovas (2000) have been used to validate the random wave propagations and dissipation over vegetation in a sloping channel based on the improved CMS-Wave model. Figure 1 shows the detailed bed elevation and the location of the vegetation. The vegetation field (artificial kelp) locates at the center of the flume and has a total width b = 7.27 m and a still water depth h = 0.77 m, the plant height was 0.20 m, the diameter of plant was 0.025 m, and the plant density was 1200 stems/m^2 (Lovas et al. 2000). The parameters of the random wave were as follows: T = 2.5 s, H_s = 0.22 m. The input for random waves is the JONSWAP spectrum from the left side boundary.

For this case, the drag coefficient of the plants has been determined using Eq. 5. Figure 2 shows comparisons of the calculated and the measured wave heights for both cases without and with vegetation. The calculated wave heights are in close agreements with the experimental data. It can be seen that the wave heights slightly increase when the waves enter the sloping bed, and then decrease because of wave breaking in the absence of plant. The wave heights have obvious attenuation at the vegetated zone as compared to that at the non-vegetated domain. The computed results show that it is reasonable to use the drag force of the vegetation as the source term in the wave action equation for investigating the interaction of wave and vegetation in the CMS-Wave model.

4.2 Solitary wave run-up and reflection on a sloping beach with and without vegetation

The processes associate with solitary wave propagation in shallow water, such as wave breaking and run-up, play an important role in the nearshore dynamics. So, solitary wave run-up on a sloping beach has been one of the most intensively studied phenomena in long-wave modeling. Laboratory experiments carried out by Synolakis (1986) provided data, which can be used to validate wave breaking and run-up simulations, as shown in Fig. 3. In Synolakis' experiment, the constant water depth was 1 m, and solitary wave height was 0.3 m. The wave propagated from left to right on a beach with a 1:19.85 slope. In this study, the HD model has been used to reproduce the wave propagation processes in Synolakis' experiment. The initial conditions include a solitary wave, propagating from left to right with the wave crest located at $X1$ (68.4 m from the left boundary). The initial solitary wave has been simulated using the solitary wave formula (Kuiry et al. 2012) as follows:

$$\eta(x,0) = H\text{sech}^2\left(\sqrt{\left(3H/(4d)\right)}(x - X_1)\right) \tag{24}$$

$$u(x,0) = \sqrt{\frac{g}{d}}\eta(x,0) \tag{25}$$

where H is the initial wave height of the solitary wave in Fig. 3.

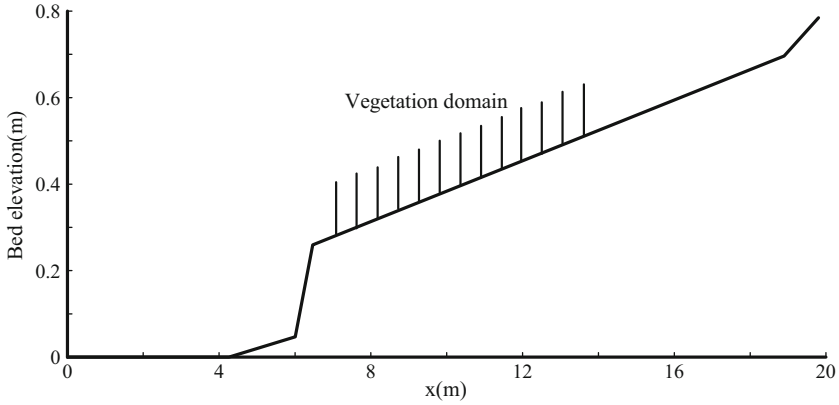

Fig. 1 Bed elevation with vegetation effect

The computation domain has been divided into cells in a uniform mesh with space steps $\Delta x = 0.1$ m, and $\Delta y = 0.1$ m. The Manning's roughness coefficient is 0.01. The simulated water surface profiles have been compared with the experimental data, for both cases with and without vegetation. In the simulations, the marsh vegetation of *Suaeda heteroptera* from Liaodong estuary is used as reference, the plant is semi-rigid, the diameter of the plants is 0.01 m, the height of the plants is 0.3 m, the density of the plants is 400 stems/m^2, and the length of plants domain is 3 m in this study. The drag force coefficient of the plant is 1.0 for the hydrodynamic model. Figure 4 shows the comparisons of the measured and computed wave profiles for both cases with and without vegetation. The water surface elevation and the length scale have been normalized by the water depth, as follows:

$$x^* = (x - x_{\text{toe}})/d \tag{26}$$

where x_{toe} is the initial location of slope's toe (73 m from the left boundary). The time scale has been normalized as follows:

$$t^* = t\sqrt{g/d} \tag{27}$$

$$\eta^* = \eta/d \tag{28}$$

t^* and η^* are non-dimensional normalized variables.

The simulated results agree very well with the experimental data at the wave crest, except for the breaking zone wave profile. As shown in Fig. 4, as the initially symmetric solitary wave shoals across the slope's toe at $x^* = 0$ m and at $t^* = 20$, it starts to form a vertical propagating face, as induced by the bottom friction and the seabed's topography. It can be seen that the simulated results have some differences at the wave crest and time scale compared to the experimental data, waves propagating the breaking zone, the present model based on shallow water equation has limitation in simulating wave dispersion, this discrepancy can be also found in other reference (Kuiry et al. 2012). The simulated water levels for the cases with and without vegetation almost coincide at $t^* = 20$; the reason for this coincidence is that the solitary wave movement has not reached the vegetated zone, and therefore, the wave propagation is not affected by the plants. At $t^* = 30$ and $t^* = 40$, the run-up heights of the solitary wave for the case with vegetation are lower than those for the case without vegetation. This is because the solitary wave loses energy as it propagates and interacts with the vegetation.

4.3 Modeling of wave height and wave-induced current in cusp vegetated channel

The beach multi-cusp bathymetry may influence rip and longshore currents developments with complex nearshore

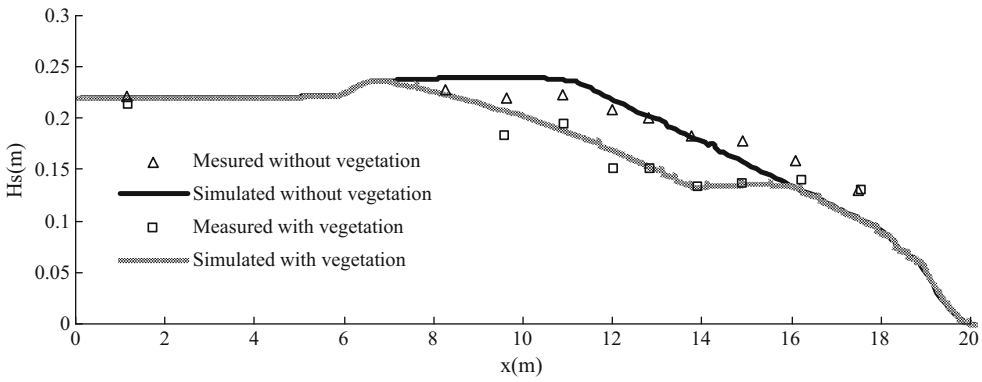

Fig. 2 Comparison of the calculated and measured wave height for breaking waves over vegetation domain

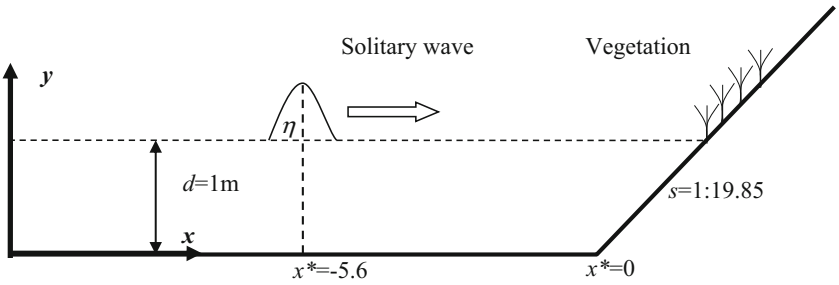

Fig. 3 Schematic of the solitary wave run-up on a sloping beach

circulation patterns owing to the interaction between waves and currents. The formed rip or longshore currents can also affect sediment transport and beach morphology along the coast. Within the UK Coastal Research Facility (UKCRF) at Wallingford, Borthwick and Foote (2002) carried out the experimental measurements of the nearshore wave-current interaction at a sinusoidal three-cusped beach. The UKCRF basin is 27 m long and 36 m wide, with a working area of 20 m by 15 m. Waves were generated with an angle from 0 to 30°. The tri-cuspate beach was situated on a 1:20 plane beach, and

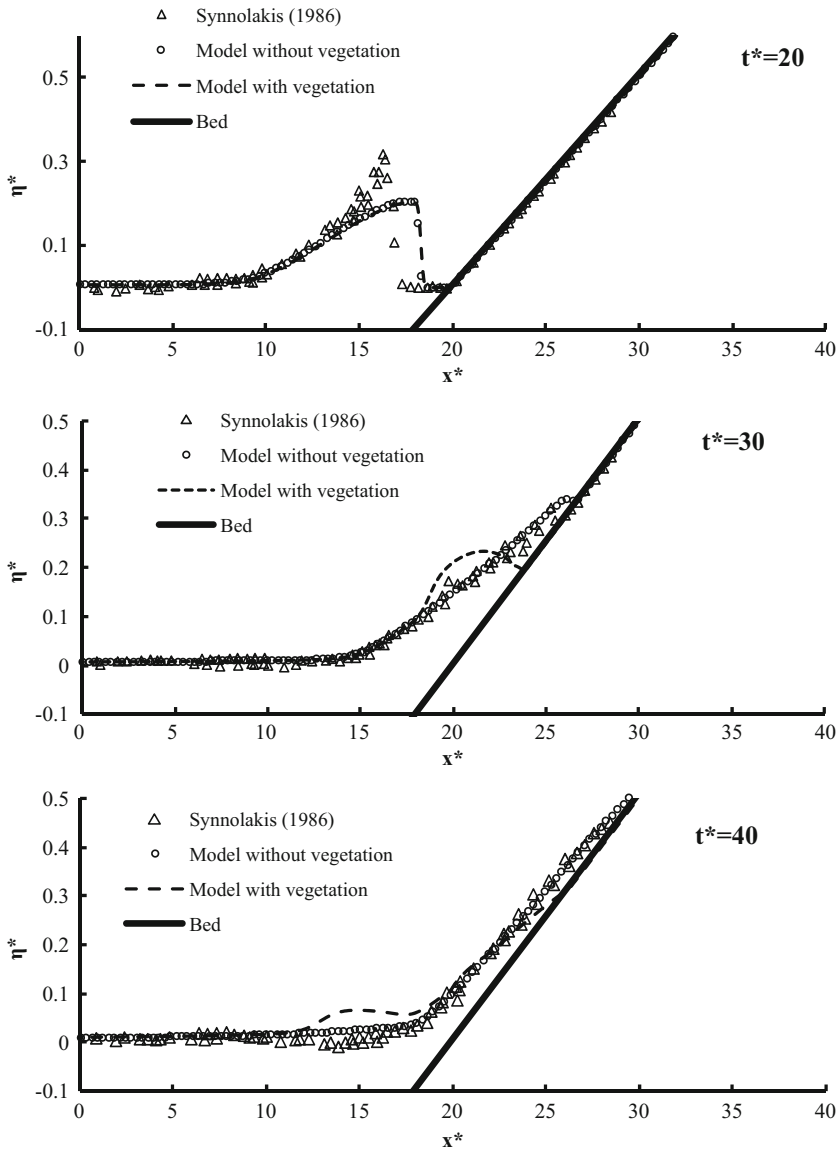

Fig. 4 Comparisons of solitary wave run-up and rundown on a 1:19.85 sloping beach

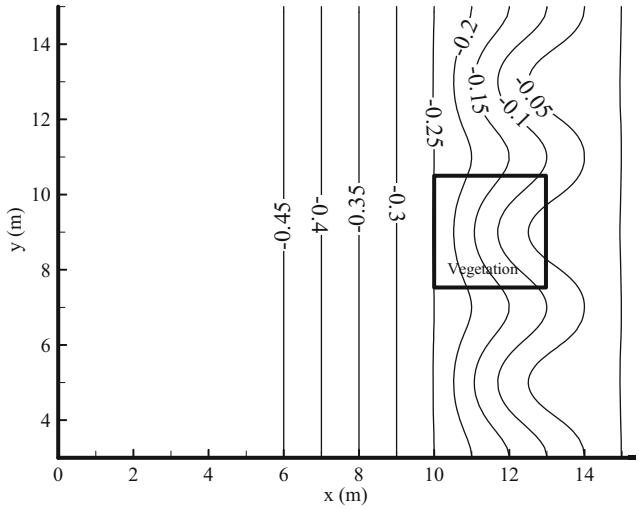

Fig. 5 Bed profile for the wave-induced current experiment

the dimensions of the plan were 12 m alongshore and 5 m onshore/offshore. At the cusps, the still water depth can be determined, as follows:

$$h(x,y) = 0.05\left((x_L - x) - 0.75\sin\left[\frac{\pi(x_L - x)}{x_L}\right]\left\{1 + \sin\left[\frac{3\pi}{2} + \frac{2\pi(y_L + y)}{R}\right]\right\}\right) \quad (29)$$

where x is the distance in the cross-shore direction, y is the distance in alongshore direction, $x_L = 5$ m is the cusp's length in cross-shore direction, and $y_L = -3$ m is the overall longshore length of the cusps, $R = 4$ m. Hence, the three cusps are located within $3 < y < 15$ m and $10\text{ m} < x < 15$ m. The bed elevation and outline of the multi-cusped beach are shown in Fig. 5.

For the oblique regular waves in case C of the UKCRF experiment, the significant wave height is 0.125 m, the wave period is 1.2 s, and the wave

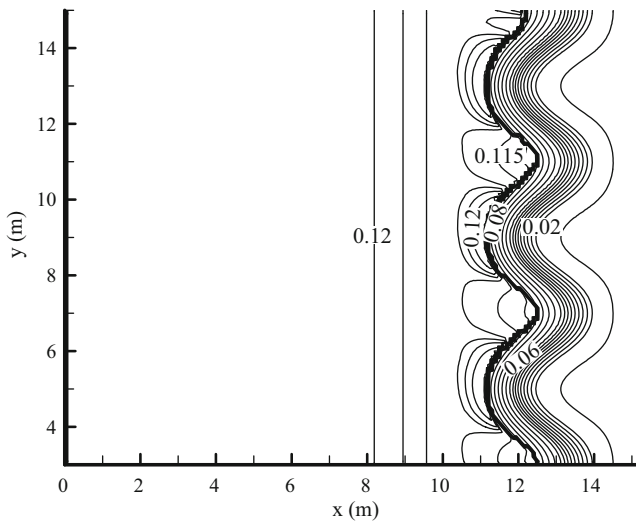

Fig. 6 Calculated significant wave height for case C of the UKCRF experiment

direction angle α is 20° with the x axis. The oblique incident waves may produce a meandering longshore current, which predominates parallel to the coastline. In this study, case C has been used to test the modeling of wave-induced currents at an idealized multi-cusped beach. A 2-D simulation has been conducted in a 16-m-long and 18-m-wide domain. A three-level quadtree mesh has been used, in which the finest grid spacing near the cusp bed is 0.125 m by 0.125 m, and the coarsest grid spacing is 0.5 m by 0.5 m outside the cusp domain. Open and still boundaries have been specified at the sea and two cross-shore boundaries; the right side of the computation domain is sloping beach. The computational time step is 0.02 s for the hydrodynamic model, and the minimum depth criterion for dry and wet bed has been set to 0.001 m, the Manning's n has been set as 0.008, and the simulation stops when the steady-state is reached. Using the coupling model, the resistance effect induced by aquatic vegetation on wave energy dissipation and hydrodynamic structure has been investigated. In the model, a finite patch of ideal vegetation, covering an area of 3 m by 3 m, has been simulated as indicated by solid lines in Fig. 5. The ideal vegetation is flexible, the plant height is 0.2 m, the diameter of plant is 0.01 m, and the density of plant is 1000 stems/m^2. The drag coefficient of the plants has been evaluated using Eq. 5 of the wave model, and it is 0.2 for flexible plant in the hydrodynamic model.

Figure 6 shows the wave height contour patterns for case C of the UKCRF experiment. It can be seen that there are slight oscillations in the wave height on the channel beach, which may be due to the reflections from the fixed cuspate beach. The incident wave accumulates and breaks before the cusped shore; the wave height contours of the broken wave spread into the embayment. Its maximum wave height in the cusp horn is approximately 1.1 times of the incident wave height in the cusp channel. Figure 7 shows the simulated spatial variability of wave radiation stresses in both x and y directions. This rapid loss in height of the broken waves may promote strong radiation stresses in the cusp channel, which in turn may create large currents. The main stress location lies in the breaking line with a water depth of 0.14 m. The longshore current pattern for the UKCRF experiment is shown in Fig. 8. It can be seen that there is a meandering longshore current in the cusp channel system driven by the oblique waves. With oscillations, it moves from left to right past the cusps, and there is a well-developed longshore current moving downwards. The simulated results by the coupling model are close to Borthwick's measured data. This shows that the coupling model can predict the longshore currents in a complex terrain. The differences between

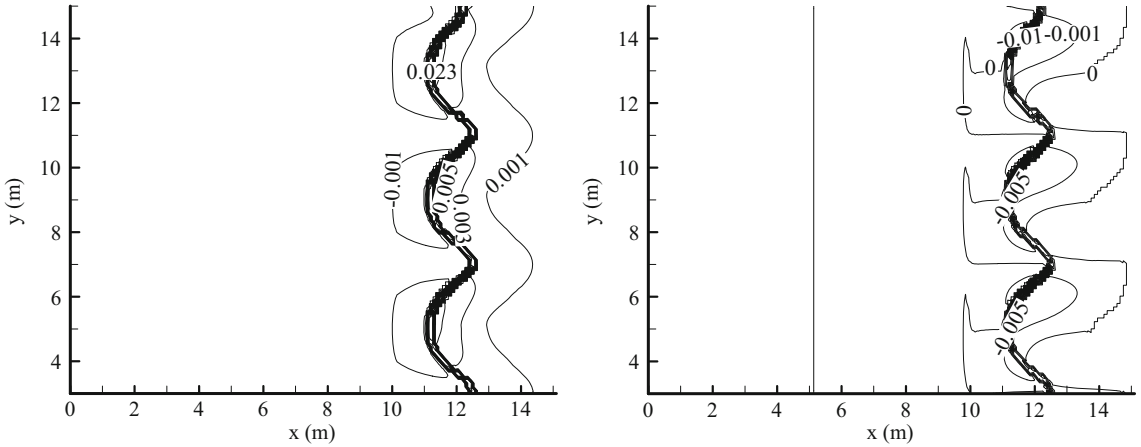

Fig. 7 Calculated wave-driven radiation stresses for case C of the UKCRF experiment

regions with and without vegetation have also been investigated in this study. In the vegetated region, as shown in Fig. 9, the wave height is greatly attenuated due to the vegetation, the reduction ratios of wave height are about 33.4% in the vegetated domain. Figure 10 shows the calculated distribution of the radiation stresses, both in x and y directions, for the case with vegetation. The radiation stress in the presence of vegetation is about 40% lower than that in the absence of vegetation. The longshore current pattern for the UKCRF experiment with vegetation is shown in Fig. 11. It can be seen that due to the presence of the vegetation, the radiation stresses are noticeably different as compared to those for the case without vegetation; the larger gradient of radiation stress forms in upwards and downwards edge of the vegetation domain. For the case with vegetation, the longshore current is reduced by the finite patch of vegetation. Further, the vegetation causes the location of the main current to shift toward the shoreline before entering the vegetated zone due to the vegetation resistance on flow; one of its important reasons also include the variations in the energy dissipation and the radiation stress in the nearshore zone.

4.4 Interaction study in co-existing environment of tides, waves, and vegetation

In recent years, researchers have paid attention to the mechanics of rip currents in experimental and numerical studies, especially under the co-existing conditions of

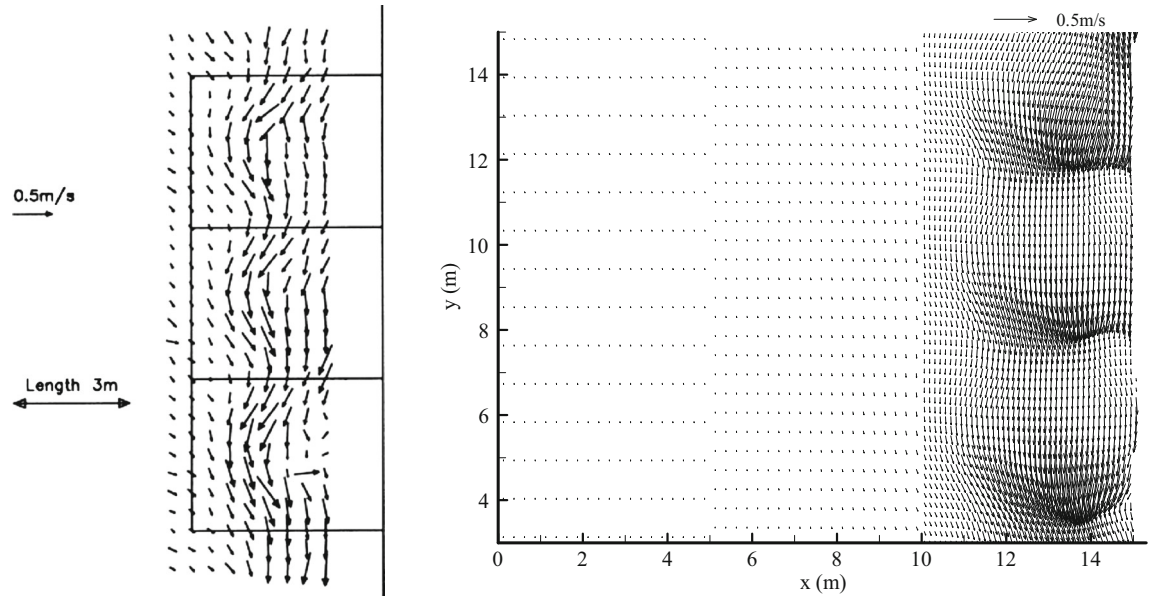

(a) Borthwick's experiment result (b) Calculated result

Fig. 8 Calculated wave-induced longshore current for case C of the UKCRF experiment

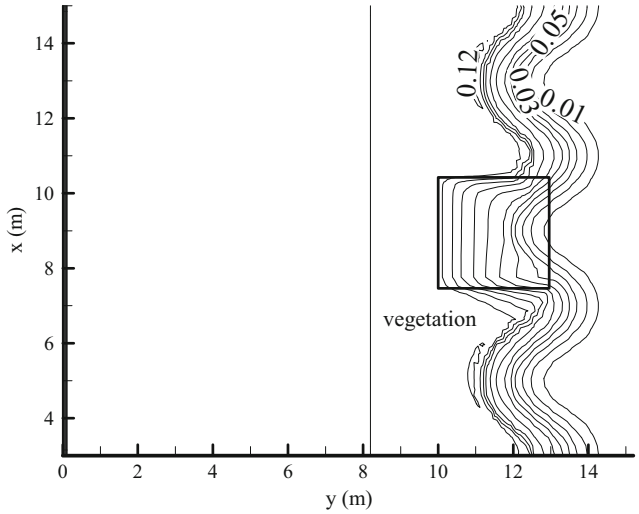

Fig. 9 Calculated significant wave height pattern for the case with vegetation

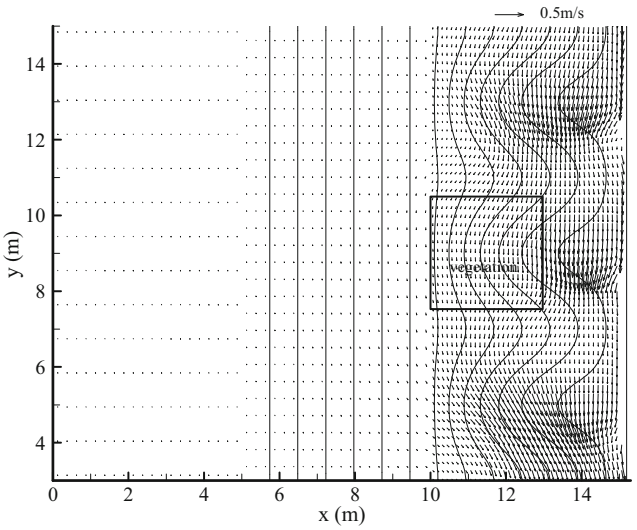

Fig. 11 Calculated wave-induced longshore current for case C with vegetation of the UKCRF experiment

waves and wave-induced currents (Park and Borthwick 2001; Borthwick and Foote 2002. However, the knowledge on the protective effect on the shoreline by coastal vegetation in the co-existing conditions of tides, waves, and vegetation is still limited. To improve the understanding of the interactions among tides, waves, and wetland plants, a numerical model of an idealized semi-closed bay with multi-cusp bed has been developed. The model can account for the effect of the wetland plant on the wave-induced currents and tides. The numerical domain of the model is 3.5 km long and 3.0 km wide. It simulates a 2-D unsteady flow driven by tidal forcing at the open boundary on the left side of the domain; an M2 tide with amplitude of 1.0 m is specified as the free surface water elevation for tidal open boundary. The rip bed is located near the center of the domain, which is similar to the UKCRF experiment (Fig. 12). The Manning's roughness coefficient for the sea bed is 0.015. The space step uses a three-level quadtree grid, in which the finest grid spacing near the rip bed is 12.5 m by 12.5 m, the coarsest grid spacing near the open boundary is 50 m by 50 m, and 25 m by 25 m inside computation domain. According to the size of the mesh and to ensure numerical stability of the model, the time step of 1 s has been selected. For this case study, the total simulated period is 72 h.

For wave simulation, the waves come from offshore (left side) with a significant wave height of 1.4 m and a wave period of 10 s in this study. Waves at zero incidence angle can generate the longshore currents which flow from cusp crests to cusp troughs, where the strong rip currents flow seaward across the surf-zone in multi-cusp bed. So, in this study, waves move at a direction of 0^{o}. In the numerical computations, both coupling models, including HD-only and HD + CMS-Wave, use

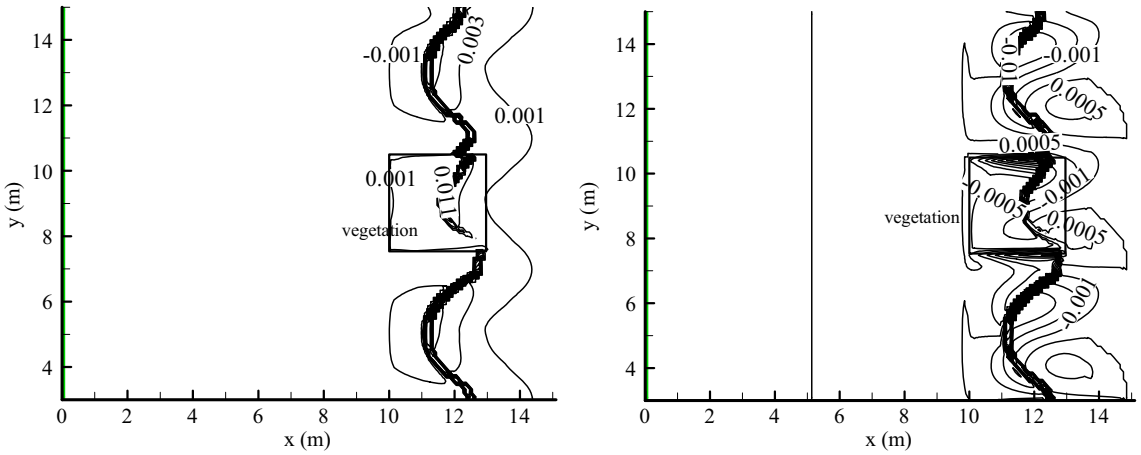

Fig. 10 Calculated wave-driven radiation stresses for the case with vegetation

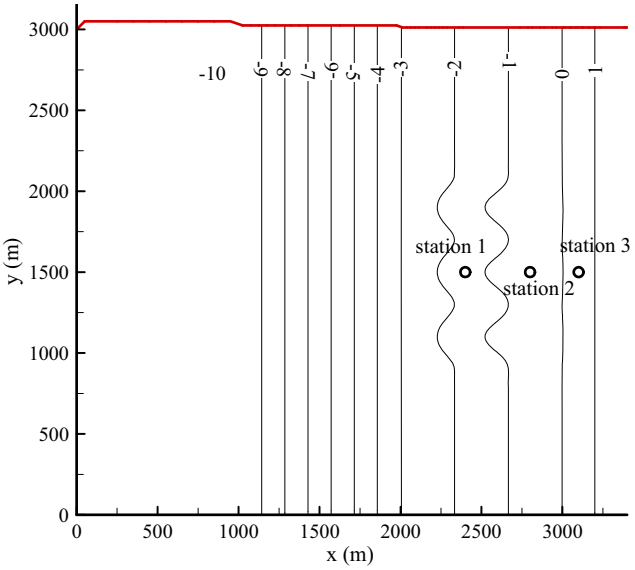

Fig. 12 Terrain contour for the rip channel system

the same set of parameters for the cases with and without vegetation so that the results can be compared directly. Stations 2 and 3 lie in the intertidal zone with complex interaction of dry and wet boundary near the coastline, as shown in Fig. 12. The time series of the water level and the depth-averaged velocity u from stations 2 and 3 are shown in Fig. 13. One case is the pure tide, and another one is the pure tide plus the effect of vegetation. The vegetation is mainly distributed in the intertidal zone ranging from 2700 to 3500 m in the x direction. It can be seen at stations 2 and 3 that the amplitudes of the water level for the case with vegetation are almost identical to those for the case without vegetation. The difference in the tide phases for with and without vegetation is due

Fig. 13 Numerically simulated water level and velocity

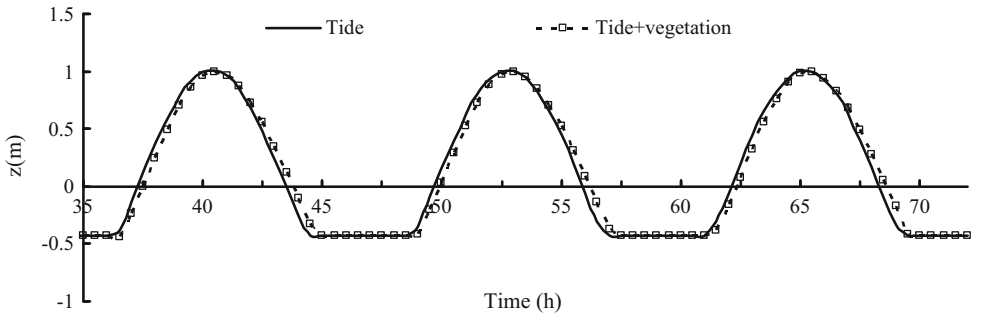

(a) station 2

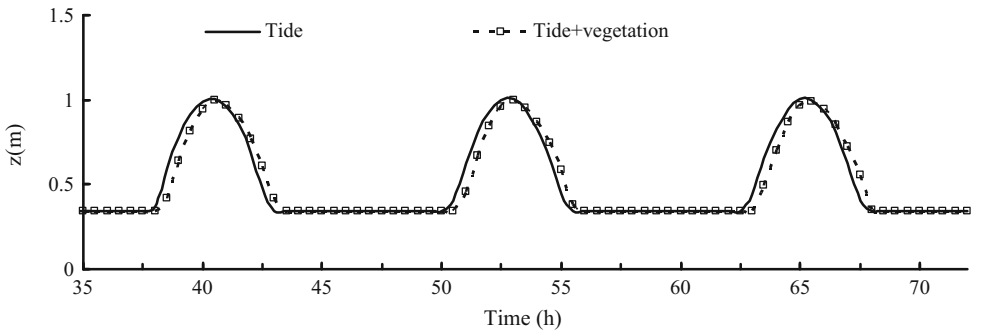

(b) station 3

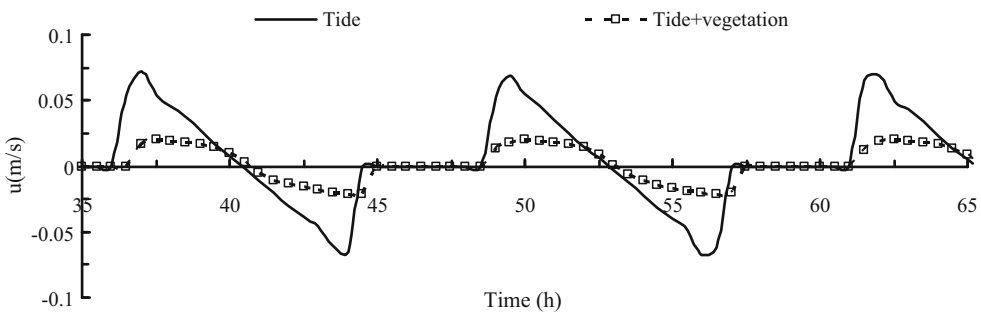

(c) station 2

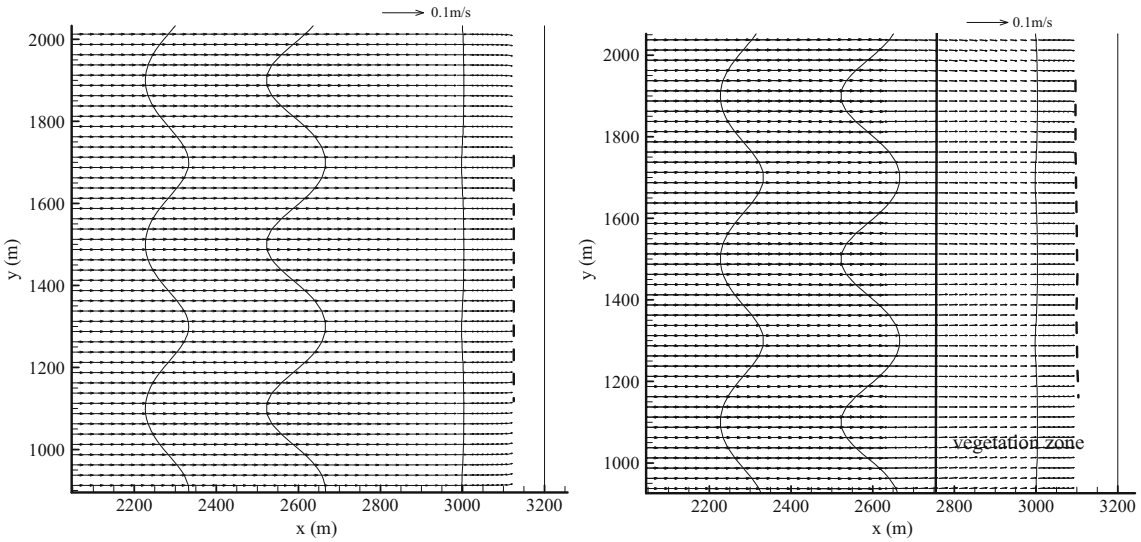

(a) at 51 h without vegetation (b) at 51 h with vegetation

Fig. 14 Numerically simulated spatial variability of current for pure tide with and without vegetation

to the variation of water level in the ebb tide, and the significant damping effects of the vegetation on velocity, which can be seen in Fig. 13c. Figure 14 shows the simulated spatial variability of the current field for the pure tide with and without vegetation, where the solid line represents bed elevation of the computation domain, dash line represents the front location of tide wave. The plant can reduce the velocity of tide wave in the vegetated domain and the run-up of water level in sloping beach with vegetation draws down as well.

Velocity and water level from the HD + CMS-Wave model for with and without vegetation at different stations are shown in Figs. 15 and 16. In station 1, the time series of the water level for the case with vegeta-

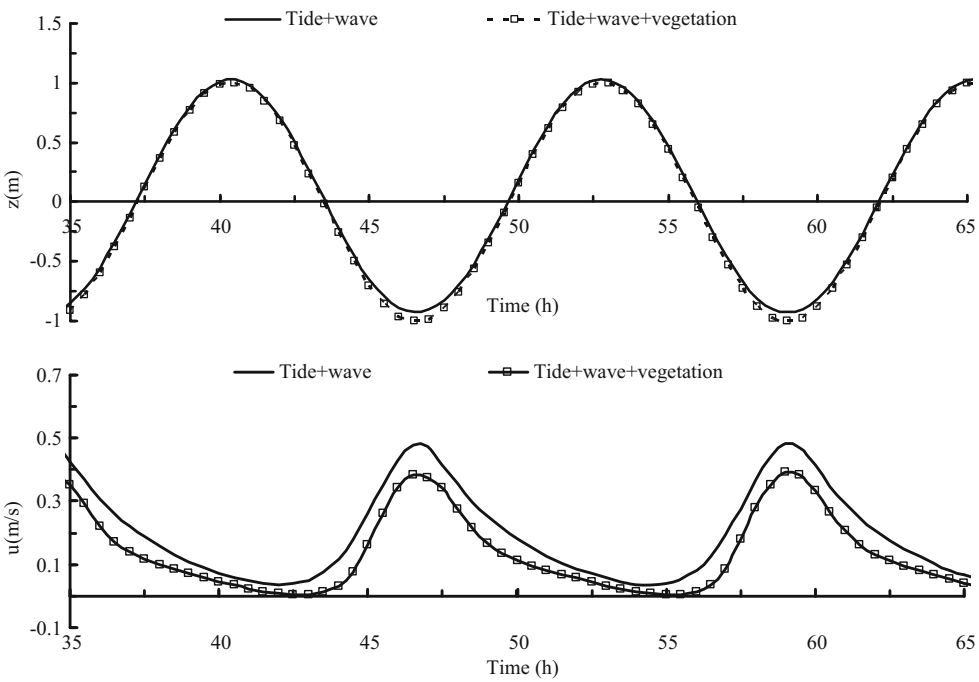

Fig. 15 Numerically simulated water level and velocity at station 1

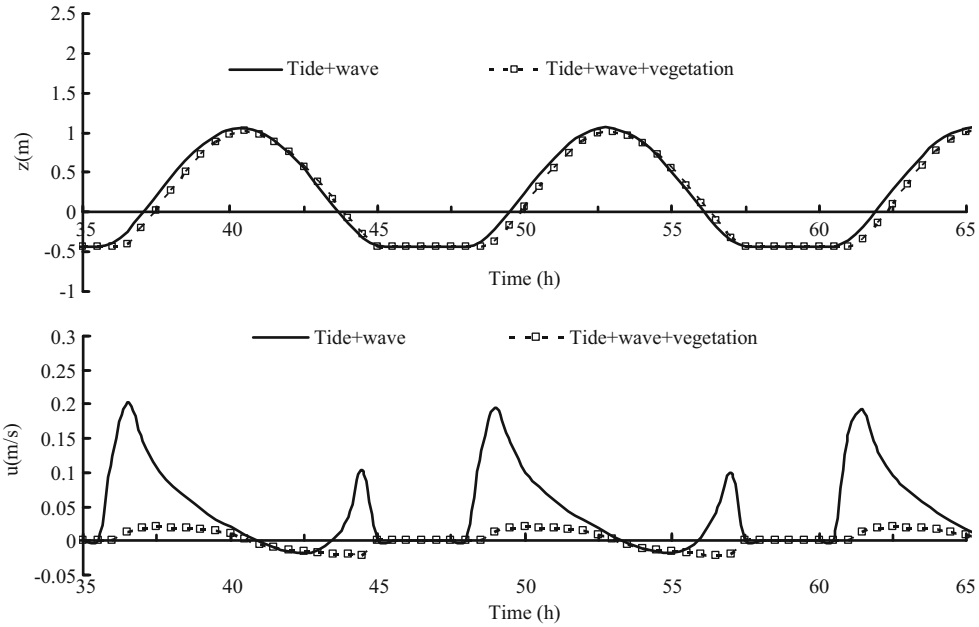

Fig. 16 Numerically simulated water level and velocity at station 2

tion are slightly lower than that for the case without vegetation in the low tide. The time series of velocity from the HD + CMS-Wave model are different as compared to those from the HD model, for both cases with and without vegetation. The positive cross-shore current induced by rip bed owing to the wave breaking is significantly larger than that of the pure tide, for both cases with and without vegetation. These results also show that the effect of the waves on rip channel behaviors is large, which means that the effect of radiation stress cannot be ignored in the study of mass and sediment transport at coastal zones. At station 2, there is no significant variation in the amplitude of water level, but the tide phase for the case with vegetation is later than that for the case without vegetation (Fig. 16). The cross-shore currents are smaller for the case with vegetation as compared to those for the case without vegetation. For both cases with and without vegetation, the currents have been analyzed in order to study the effect of vegetation on the circulation in the ebb tide at 46 h and in the flooding tide at 51 h. Because flow resistance caused by vegetation is proportional to the velocity squared, it can be seen that wetland vegetation is most efficient at dissipating momentum in areas of stronger currents or including the wave-induced current. Figure 17 shows the clockwise and anticlockwise rotating circulations. The generation of the closed circulation cells is favored under such conditions of zero angle incidence wave and multi-cusp bed vegetation of intertidal zone can impact the current process. An example of the radiation stress field (x direction) during the flooding and ebb tides is shown in Fig. 18. The radiation stress in this computation domain is mainly distributed alongshore, and its magnitude is small at areas far away from the coast. During the ebb tide in Fig. 18a, the negative tide levels occur with the dry domain along the coast; wave breaking occurs early when waves reach the rip bed with breaker criterion for the combined effects of current, depth with bottom slope. The location of radiation stress in the x-direction moves toward the shoreline because of the water depth variation during the positive flooding tide levelsin Fig. 18b.

5 Conclusions

A depth-averaged coupling model of tide and wave has been developed, which can simulate the flow phenomena and wave height variation for coastal waters in the presence of wetland plants. The equations in the hydrodynamic model are solved by using an explicit finite volume method with HLL approximate Riemann solver for flux terms based on quadtree mesh. The model also considers all the physical forces such as earth rotation, bed friction, and wave radiation stress. The spectral wave action model is based on a wave action balance equation with vegetation effect, which can simulate the

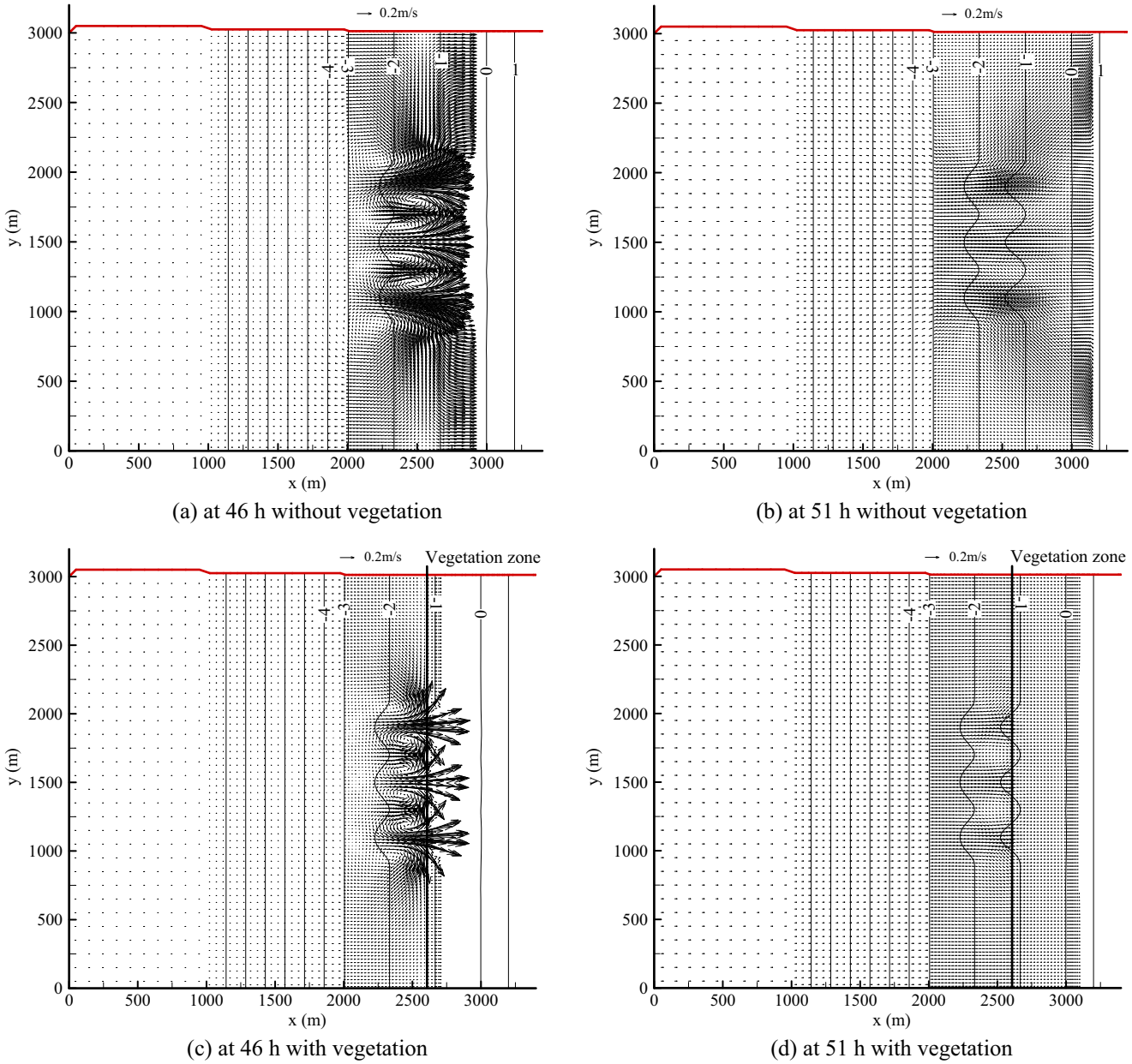

Fig. 17 Numerically simulated current with flooding and ebb tides with wave effect

wave propagation by accounting for wave breaking, shoaling, refraction, diffraction, wind effect, and current effect in coastal wetland zones.

Several cases have been selected to validate the wave and tide models in vegetated sloping beds. The calculated results show that it is reasonable to represent the resistance induced by aquatic plants in the CMS-Wave model by adding a wave energy dissipation term in the wave action balance equation. The calculated results show that the wave height decay follows the same trends in all the cases due to the vegetation resistance effect on the breaking waves. The model results also show that the plant can significantly affect the solitary wave transmission and run-up on a sloping bed.

The simulation results show that wave angle and the embayment size are crucial to rip channel dynamics on embayed beaches. As the currents and wave heights interact with each other in the rip channel system, the variations in the wave heights in the rip channel system may induce alongshore currents generated by the oblique incident waves. For co-existing environment of wave and current, the plant effects on wave-induced

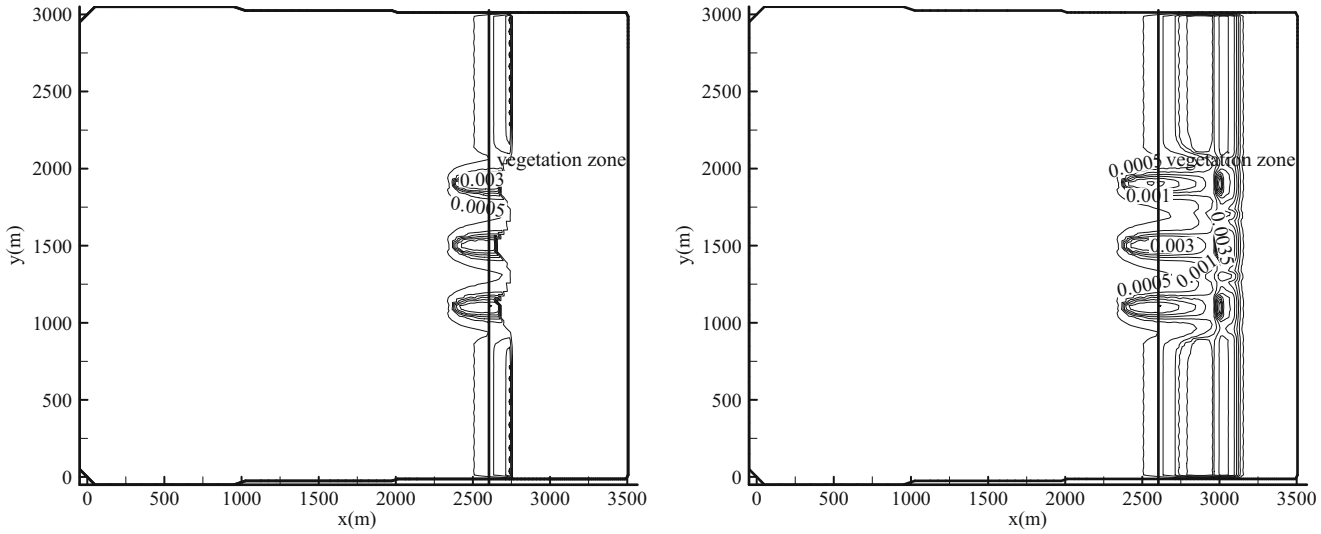

Fig. 18 Numerically simulated spatial variability of wave-induced radiation stress with flooding and ebb tides

currents depend on the vegetation resistance, the variation of the energy dissipation, and the radiation stress in the vegetation zone, which tend to slow down the current in the region with vegetation and shift the main current in the vicinity of the vegetation.

The clockwise and anticlockwise rotating circulation can occur under the rip channel system due to the vertical incident wave for tide and wave in the co-existing environment. The computed results also show that the effect of the wave on the rip channel behavior is large in the nearshore domain, which means that the effect of radiation stress cannot be ignored in the study of mass and sediment transport at coastal zones. It is noted that the structure of the rip velocity varies with tide and vegetation. Mean cross-shore velocity always becomes slower due to the vegetation. Changes in the water level affect how far the wave breaking can extend into the channel; the location of radiation stress moves toward shoreline and offshore because of the water depth variation during the flooding tide and ebb tide.

It has been demonstrated that the coupled model can simulate the interactions among wave-currents, tides, and wetland plants in wetland waters, especially in the dry and wet discontinuous flow condition, which can improve the simulation results of waves and wave-induced currents during tidal processes in wetland waters.

Acknowledgements This work was supported by the National Nature Science Foundation of China (51579030), the Wetland Degradation and Ecological Restoration Program of Panjin Pink Beach (PHL-XZ-2017013-002), the Liaoning Natural Science Foundation (2014020148), the Open Fund of the State Key Laboratory of Hydraulics, and Mountain River Engineering (SKHL1517).

References

Anderson ME, Smith JM (2014) Wave attenuation by flexible, idealized salt marsh vegetation. Coast Eng 83:82–92

Augustin LN, Irish JL, Lynett P (2009) Laboratory and numerical studies of wave damping by emergent and near-emergent wetland vegetation. Coast Eng 56:332–340

Blackmar PJ, Cox DT, Wu W (2014) Laboratory observations and numerical simulations of wave height attenuation in heterogeneous vegetation. J Waterw Port Coast Ocean Eng 140:56–65

Blumberg AF (1994) A primer for ECOM-si, technical report. HydroQual, Mahwah

Booij N, Ris RC, Holthuijsen LH (1999) A third-generation wave model for coastal regions, part I, model description and validation. J Geophys Res 104(C4):7649–7666

Borthwick AGL, Foote YLM (2002) Wave-induced nearshore currents at a tri-cuspate beach in the UKCRF. Water Mar Eng 4:251–263

Buttolph AM, Reed CW, Kraus NC, Ono N (2006) Two-dimensional depth-averaged circulation model CMS-M2D: version 3.0, report 2, sediment transport and morphology change. Technical Report ERDC/CHL TR-06-9, Coastal and Hydrodynamics Laboratory, US Army Corps of Engineers, Vicksburg, MS, USA

Chen Q, Zhao HH (2012) Theoretical models for wave energy dissipation caused by vegetation. J Eng Mech 138(2):221–229

Chen CS, Gao GP, Zhang Y, Beardsley RC, Lai ZG, Qi JH, Lin HC (2016) Circulation in the Arctic Ocean: results from a high-resolution coupled ice-sea nested global-FVCOM and Arctic-FVCOM system. Prog Oceanogr 141:60–80

Dalrymple RA, Kirby JT, Hwang PA (1984) Wave diffraction due to areas of energy dissipation. J Waterw Port Coast Ocean Eng 110:67–79

Das S, Crépin AS (2013) Mangroves can provide protection against wind damage during storms. Estuar Coast Shelf Sci 134:98–107

Dietrich JC, Tanaka S, Westerink JJ, Dawson CN, Luettich RAJ, Zijlema M, Holthuijsen LH, Smith JM, Westerink LG, Westerink HJ (2012) Performance of the unstructured mesh SWAN+ADCIRC model in computing hurricane waves and surge. J Sci Comput 52(2):468–497

Ding Y, Kuiry SN, Elgohry M, Jia YF, Altinakar MS, Yeh KC (2013) Impact assessment of sea-level rise and hazardous storms on coasts and estuaries using integrated processes model. Ocean Eng 71:74–95

Dubi A, Torum A (1997) Wave energy dissipation in kelp vegetation. In: Edge BL (ed) Proceedings of the Twenty-Fifth Coastal Engineering Conference. Am Soc of Civil Eng, New York, pp 2626–2639

Feagin RA, Irish JL, Möller I, Williams AM, Colón-Rivera RJ, Mousavi ME (2011) Short communication: engineering properties of wetland plants with application to wave attenuation. Coast Eng 58:251–255

Hansen JE, Raubenheimer B, List JH, Elgar S (2015) Modeled alongshore circulation and force balances onshore of a submarine canyon. J Geophys Res 120(3):1887–1903

Hu Z, Suzuki T, Zitman T, Uittewaal W, Stive M (2014) Laboratory study on wave dissipation by vegetation in combined current-wave flow. Coast Eng 88:131–142

Irtem E, Gedik N, Kabdasli MS, Yasa NE (2009) Coastal forest effects on tsunami run-up heights. Ocean Eng 36(3–4):313–320

Kaveh NA, Ghaheri A, Chegini V, Nazarali M (2016) Application of a hybrid approach for tide-surge modeling in the Persian Gulf. J Coast Res 32(5):1126–1134

Kuiry SN, Wu WM, Ding Y (2012) A one-dimensional shock-capturing model for long wave run-up on sloping beaches. J Hydraul Eng 18(2):65–79

Kumar N, Voulgaris G, Warner JC, Olabarrieta M (2012) Implementation of the vortex force formalism in the coupled ocean-atmosphere-wave-sediment transport (COAWST) modeling system for inner shelf and surf zone applications. Ocean Model 47:65–95

Lawler S, Haddad J, Ferreira CM (2016) Sensitivity considerations and the impact of spatial scaling for storm surge modeling in wetlands of the Mid-Atlantic region. Ocean Coast Manag 134:226–238

Li CW, Yan K (2007) Numerical investigation of wave-current-vegetation interaction. J Hydraul Eng 133(7):794–803

Lin L, Demirbilek Z (2005) Evaluation of two numerical wave models with inlet physical model. J Waterw Port Coast Ocean Eng 131(4): 149–161

Lin LH, Demirbilek Z, Mase H, Zheng JH (2008) CMS-wave: a nearshore spectral wave processes model for coastal inlets and navigation projects. Technical Report ERDC/CHL TR-08-13, Coastal and Hydrodynamics Laboratory, ERDC, US Army Corps of Engineers, Vicksburg, MS, USA

Loder N, Irish JL, Cialone M, Wamsley T (2009) Sensitivity of hurricane surge to morphological parameters of coastal wetlands. Estuar Coast Shelf Sci 84:625–636

Lovas SM (2000) Hydro-physical conditions in kelp forests and the effect on wave damping and dune erosion: a case study on *Laminaria hyperborea*. PhD thesis, University of Trondheim, The Norwegian Institute of Technology, Trondheim, Norway

Luettich RA, Westerink JJ, Scheffner NW (1992) ADCIRC: an advanced three dimensional circulation model for shelves, coasts, and estuaries, Report 1, Theory and methodology and ADCIRC-2DDI and ADCTRC-3DL. Tech. Rep. DRP-92-6, US Army Engineering Waterways Experiment Station, Vicksburg

Ma GF, Kirby JT, Su SF, Figlus J, Shi FY (2013) Numerical study of turbulence and wave damping induced by vegetation canopies. Coast Eng 80:68–78

Marsooli R, Wu W (2014) Numerical investigation of wave attenuation by vegetation using a 3D RANS model. Adv Water Resour 74:245–257

Mase H (2001) Multidirectional random wave transformation model based on energy balance equation. Coast Eng 43(4):317–337

Maza M, Lara JL, Losada IJ, Ondiviela B, Trinogga J, Bouma TJ (2015) Large-scale 3-D experiments of wave and current interaction with real vegetation. Part 2: experimental analysis. Coast Eng 106:73–86

Maza M, Lara JL, Losada IJ (2016) Solitary wave attenuation by vegetation patches. Adv Water Resour 98:159–172

Méndez FJ, Losada IJ (2004) An empirical model to estimate the propagation of random breaking and nonbreaking waves over vegetation fields. Coast Eng 51:103–118

Moller I, Spencer T, French JR, Leggett DJ, Dixon M (1999) Wave transformation over salt marshes: a field and numerical modelling study from North Norfolk, England. Estuar Coast Shelf Sci 49:411–426

Park KY, Borthwick AGL (2001) Quadtree grid numerical model of nearshore wave–current interaction. Coast Eng 42:219–239

Qi JH, Chen CS, Beardsley RC (2009) An unstructured-grid finite-volume surface wave model (FVCOM-SWAVE): implementation, validations and applications. Ocean Model 28:153–166

Sanchez A, Wu WM, Beck TM (2016) A depth-averaged 2-D model of flow and sediment transport in coastal waters. Ocean Dyn 66:1475–1495

Suzuki T, Zijlema M, Burger B, Meijer MC et al (2012) Wave dissipation by vegetation with layer schematization in SWAN. Coast Eng 59(1): 64–71

Synolakis CE (1986) The run-up of long waves. PhD Thesis, California Institute of Technology, Pasadena

Toro EF (2001) Shock-capturing methods for free-surface shallow flows. Wiley, New York

Turker U, Yagci O, Kabdasl MS (2006) Analysis of coastal damage of a beach profile under the protection of emergent vegetation. Ocean Eng 33:810–828

Wang HJ, Wang AM, Bi NS, Zeng XM, Xiao HH (2014) Seasonal distribution of suspended sediment in the Bohai Sea, China. Cont Shelf Res 90:17–32

Warner JC, Armstrong B, He RY, Zambon JB (2010) Development of a coupled ocean–atmosphere–wave–sediment transport (COAWST) modeling system. Ocean Model 35:230–244

Zeng XM, He RY, Zuo X, Wang HJ, Wang Y, Yao ZG, Guan WB, Warrillow J (2015) River-derived sediment suspension and transport in the Bohai, Yellow, and East China Seas: a preliminary modeling study. Cont Shelf Res 111:112–125

Zhang ML, Wu WM, Lin LH, Yu JN (2012) Coupling of wave and current numerical model with unstructured quadtree grid for nearshore coastal waters. Sci China Technol Sci 55(2):568–580

Zhang ML, Hao ZN, ZhangYP WWM (2013) Numerical simulation of solitary and random wave propagation through vegetation based on VOF method. Acta Oceanol Sin 32(7):38–46